VOL. 12, NO. 7, APRIL 2017 ISSN 1819-6608
ARPN Journal of Engineering and Applied Sciences

www.arpnjournals.com

ON AMORPHOUS PHASE FORMATION IN DISSIMILAR FRICTION STIR WELDING OF ALUMINIUM-TO-STEEL

Sadiq Aziz Hussein[1] and Abd Salam Md Tahir[2]
[1]Technical Instructor Training Institute, Middle Technical University, Baghdad, Iraq
[2]Faculty of Mechanical Engineering, UniversitiTeknikal Malaysia Melaka (UTeM), Melaka, Malaysia
E-Mail: dr.sadiq@mtu.edu.iq

ABSTRACT

The amorphous phase which associated the joining of aluminium-to-steel via friction stir welding was investigated. AA5083, AA6061 and zinc coated steel were welded together by a single pass friction stir welding. Heat cycle measurement and scanning electron microscopy were conducted to investigate the effect of using different welding parameter levels on the amorphous phase and intermetallic compound formations. Using of 2000 rpm with 20 mm/min as rotational and welding speeds, respectively, resulted in a long heat cycle. Such long heat cycle could eliminate the amorphous phase and promote thick intermetallic compounds, especially at the AA5083 to steel interface. However, when welding speed was increased, 40 mm/min, a shorter heat cycle was produced, and the amorphous phase was observed. Very high welding speed (300 mm/min) resulted in very short heat cycle with no obvious amorphous phase and very small amount of intermetallic compound at the aluminium-to-steel interface. The formation process of the amorphous phase is schematically explained in this study.

Keywords: FSW, dissimilar welding, aluminium-to steel, intermetallic compound, amorphous phase.

1. INTRODUCTION

Design that produces light weight, high strength, optimum topological structure and low fuel consumption of transports applications is a never-ending desire. Structure made from multi-materials (Bimetal, Trimetal, and Tetrametal) represents one of the best compromise solutions. The integrated structures of steel and aluminium are widely used to attain high strength to weight ratio in transport applications [1]. However, efficient joining method of aluminium-to-steel (Al-to-steel) is a critical issue in producing such hybrid structure. The difficulty of joining Al-to-steel using fusion welding methods is related to the advanced differences in melting temperature, thermal properties, cooling rate after welding of both metallic alloys and promotion of thick intermetallic compound (IMC). Though, friction stir welding (FSW) can achieve efficient joint strength of such metallic alloys due to its solid state behaviour, it also promotes IMC at the Al-to-steel interface [2].

Several researches have been conducted to characterize the IMC of the Al-to-steel joint made by FSW. Springer *et al* [3] stated that the pre-deformation of the parent materials caused by the FSW process will have pronounced effect on the composition and growth of the IMC layer, in which an amorphous phase is formed before the IMC layer formation. Ogura *et al* [4] who noticed this amorphous phase stated that the amorphous phase is most likely a kneading stage that leads to the IMC formation when the applied heat is sufficient. Sun *et al* [5] emphasized that the amorphous phase is caused mainly by mechanical alloying during the excessive plastic deformation, and not because of a thermally driven mechanism. They are convinced that the formation of IMCs is a thermally driven diffusion process. It is clear from the addressed literature that IMC is formed in the Al-to-steel joint made by FSW [6, 7]. Besides, an amorphous phase might also be formed before the IMC presence [4]. Very few studies discussed this amorphous phase, which implies more investigations that can explain the influential parameter on such phase.

In this study, a trial had been made to explain this amorphous phase and the affected welding process parameters. Besides, the joining of different types of aluminium alloys by single pass FSW could add further significant data to the outcomes of this study.

2. EXPERIMENTAL WORKS

The workpieces materials were 3 mm thick AA5083-H112, AA6061-T6 sheets and 1.5 mm thick zinc-coated-steel sheet. The compositions of these metallic alloys per the manufacturer's data sheet are shown in Table-1. Vertical CNC milling machine (HASS VF-1D) was used. The arrangement of the plates is shown in Figure-1. The welding tool made from tungsten carbide and tool steel-H13 is shown in Figure-2. Tool shoulder was dipped into the workpieces by 0.3 mm to insure the contact incidents between the tool and the workpieces. The pin tip was not plunged into the steel plate. The welding parameters are shown in Table-2. The rotational and downward speeds during the plunging stage were 1000 rpm and 5 mm/min, respectively, which could avoid incoming high forces [8]. Heat cycle was measured experimentally at the Al-to-steel interface by using a USB TC-08 thermocouple (range of 0–1820 °C) with 8-port capacity, as shown in Figure-1. Scanning electron microscopy (SEM) was then used to investigate the amorphous phase and IMC formations at the weld interface microstructure. The microstructure samples were prepared for the microstructure tests by cold mounting to avoid associated incoming heat during the hot mounting process. The surfaces were grinding with abrasive paper grit 500 and 1200, and then polished with 9, 6, 3 and 1 μm diamond suspensions.

Table-1. Chemical and mechanical properties of the materials.

Material	Chemical composition wt.%	Actual UTS (MPa)
AA5083-H112	0.08 Si, 0.27 Fe, 0.03 Cu, 0.65 Mn, 4.71 Mg, 0.08 Cr, 0.04 Zn, 0.02 Ti, balance Al	313
AA6061-T6	0.67 Si, 0.32 Fe, 0.32 Cu, 0.014 Mn, 1.06 Mg, 0.21 Cr, 0.007 Zn, 0.02 Ti, other 0.05, balance Al	299
Zinc-coated-steel (JIS G3313)	0.0204 C, 0.027 Si, 0.199 Mn, 0.0079 P, 0.0083 S. Zinc coated weight is 19 g/m^2 on both surfaces	282
Note: The ultimate tensile strength (UTS) of this table is the average of four tested samples for each tabulated material.		

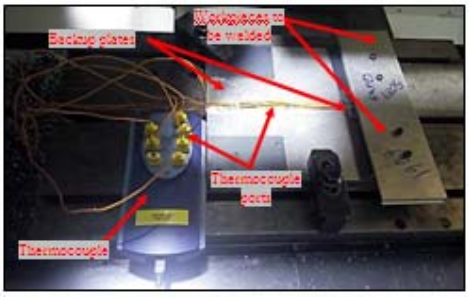

(a)

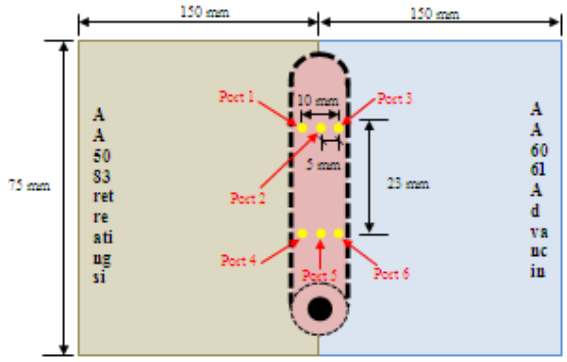

(b)

Figure-1. Experimental setup (a) the workpieces fixture and the CNC table (b) schematic diagram of the thermocouple ports positions at the Al-to-steel interface.

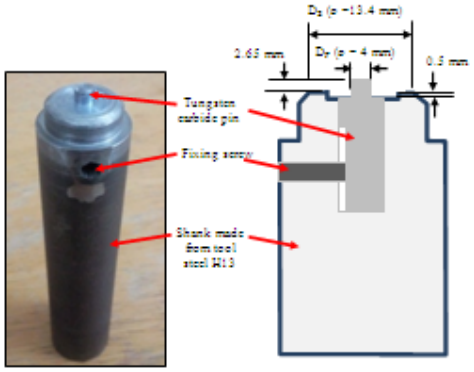

Figure-2. Design specification of the FSW tool.

Table-2. The welding parameters.

Rotational speed (rpm)	Welding speeds (mm/min)
1800	20, 300
2000	20, 40, 300

3. RESULTS AND DISCUSSIONS

Rotational speed (N) and welding speed (v) affected the heat cycle (thermal history) of the weld. Peak temperature (Tp) of welding process when N = 1800 rpm (Figure-3) was lower than the Tp when N = 2000 rpm (Figure-4). It is well known that increasing N factor will lead to an increase in the heat input [9]. Contrarily, Figures 3 and 4 show that Tp decreased with an increase in the welding speed, i.e. 20 mm/min provided higher weld temperature as compared to 300 mm/min. A large difference in welding speed tends to reduce the heat input to the workpieces during the FSW process [10]. This phenomenon is related to the long frictional time, and high plastic deformation occurred along the welding line [11]. This welding speed significantly affected the cooling rate of the heat cycles (Figures 3 and 4) as well. In other words, low welding speed (such as 20 mm/min) showed a longer time for the workpiece to be under hot condition.

Due to the differences in materials flow, the temperature distribution is asymmetric as claimed by Jacquin et al [11]. The temperature distributions at the advancing side (AS) and retreating side (RS) are explained in Figures 3 and 4). Nandan *et al* [12] and Rao *et al* [14] stated that pin rotation and welding direction would be similar on the AS and opposite on the RS of the weld. Therefore, high heat is concentrated at the high flow of metal region (AS) because of high plastic deformation [12, 14]. In the present study, the hotter zone was at AS when the welding speed was 20 mm/min. However, this was not occurred when the welding speed was very high (300 mm/min). It is most likely that this temperature distribution was affected by the rate of welding speed and weld pitch (rev/mm). The high weld pitch might not provide enough time to stabilize the temperature, especially, with the dissimilarities in the properties of the welded Al Alloys, such as thermal conductivity which affected by the temperature rise.

Consequently, heat amount and tool duration at each point along the weld line were very important factors in this heat distribution issue. The heat cycle of 2000 rpm with 40 mm/min shown in Figure-5 resulted in shorter heat cycle compare to 2000 rpm with 20 mm/min, but longer than 2000 rpm with 300 mm/min.

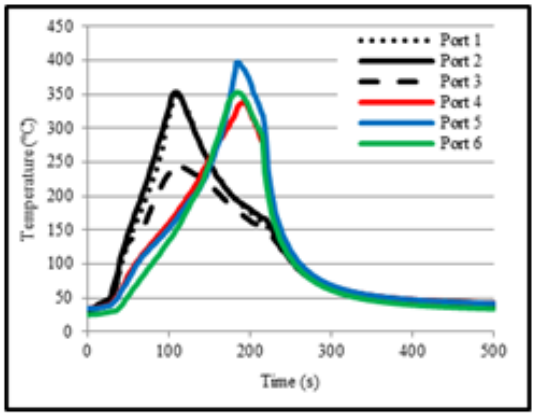

(a)

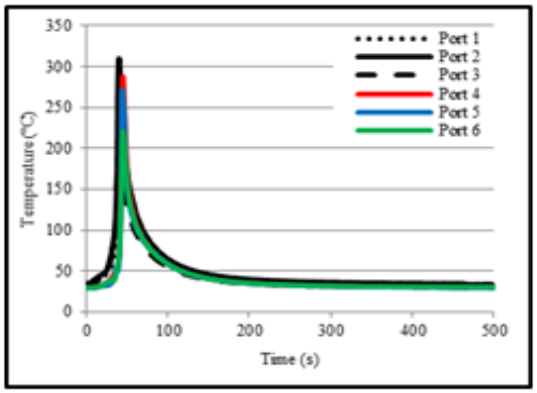

(b)

Figure-3. Heat cycle of weld made by 1800 rpm with (a) 20 mm/min, (b) 300 mm/min.

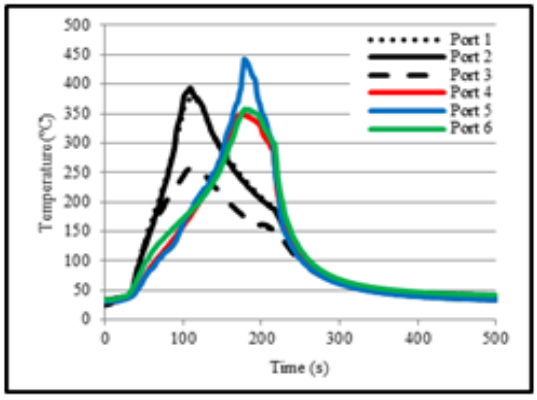

(a)

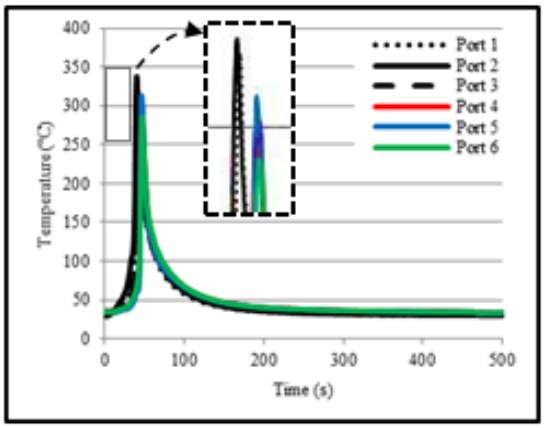

(b)

Figure-4. Heat cycle of weld made by 2000 rpm with (a) 20 mm/min, (b) 300 mm/min.

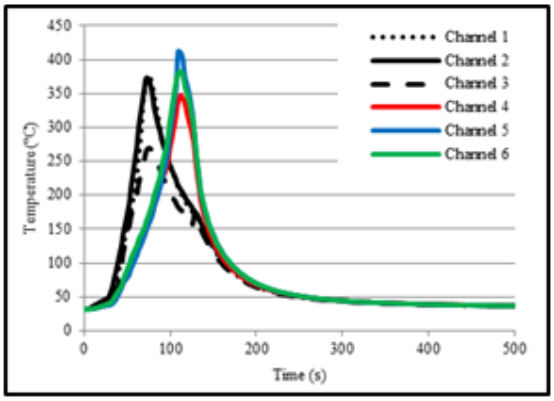

Figure-5. Heat cycle of weld made by 2000 rpm with 40 mm/min.

During the microstructure investigation, the weld made by using high welding speed 300 mm/min did not show a noticeable amorphous phase, and very small discontinuous IMC layer could be observed, as shown in Figure-6. Besides, no obvious amorphous phase could be noticed at the Al-to-steel interface when 20 mm/min was used and for both rotational speeds, as shown in Figure-7. IMC layer was formed at both sides with different thicknesses. In general, these IMCs were thick at the AA5083 side in which showed some cracks, while AA6061 side promoted thin free of cracks layer for the case of v = 20 mm/min. Furthermore, it was very difficult to find when v = 300 mm/min.

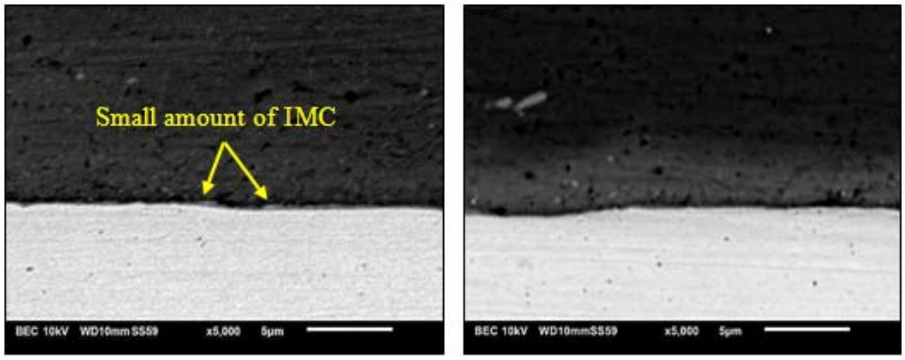

Figure-6. Very small amount of the IMC at the AA5083-to-steel side for weld made by using v = 300 mm/min.

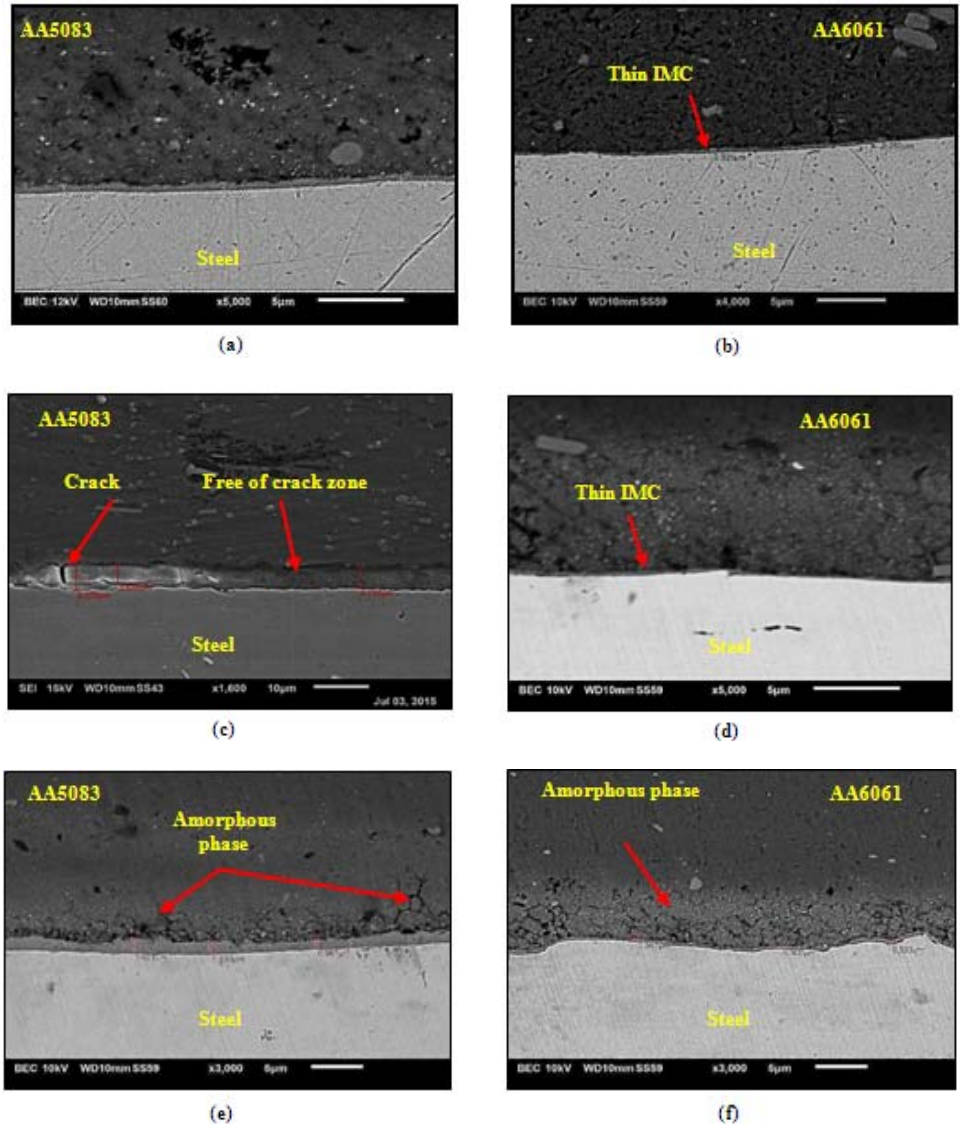

Figure-7. Al-to-steel interfaces for different welding parameters at both dissimilar Al Alloys (a) N = 1800 rpm with v = 20 mm/min AA5083-to-steel, (b) N = 1800 rpm with v = 20 mm/min AA6061-to-steel side. (c) N = 1800 rpm with v = 20 mm/min AA5083-to-steel, (d) N = 2000 rpm with v = 20 mm/min AA6061-to-steel side, (e) N = 2000 rpm with v = 40 mm/min AA5083-to-steel, and (f) N = 2000 rpm with v = 40 mm/min AA6061-to-steel side.

The peak temperature of port 5 and the cooling time of the heat cycle measurement were lower when v = 40 mm/min was used as compared to 20 mm/min. This difference in the heat cycle promoted amorphous phase and thinner IMC layer thickness was formed. The temperature at the AA6061 side was higher than the temperature at the AA5083 for the rotational speed of 2000 rpm with 20 and 40 mm/min as welding speeds. This was significant observation as AA5083 promoted thick IMC than the AA6061 though the lower temperature at that side. This phenomenon can be related to the Si presence at the AA6061 plate. Kobayashi and Yakou [13] believed that IMC layer is inhibited by the existence of Si atoms which are higher in AA6061 material as compared to the AA5083 one (Table-1). Cracks were found at the Al-to-steel interface (Figure-7-c), which denoted a deleterious effect on the joint strength. Hot and long heat cycle led to thick IMC when N = 2000 rpm and v = 20 mm/min were used.

In Figure-7 (e and f), an amorphous phase is clearly shown. The increase of welding speed leads to lower plastic deformation [15]. Therefore, 40 mm/min led to lower plastic deformation than that obtained by using 20 mm/min. On the other side, increasing the rotational speed will increase the plastic deformation. It is believed that increasing the heat cycle could help the transformation of this amorphous phase to the IMC phase, which would further increase the layer thickness [5]. When welding speed was set to 20 mm/min, no obvious amorphous phase was detected because of the long heat cycle. It is worthy to mention that excessive plastic deformation could be achieved by considering other parameters such as threaded pin profile or big tool size [4]. Therefore, high plastic deformation together with low heat cycle condition (2000 rpm, 40 mm/min), were likely to be the main cause of this phase existence. When plastic deformation and heat cycle were high (2000 rpm, 20 mm/min) this phase was not observed. Setting N = 2000 rpm with v = 300 mm/min produced lower heat cycle and plastic deformation, and thereby no amorphous phase was detected though very small IMC was observed. The AS was subjected to more plastic deformation, which induced more amorphous phase amount on this side (Figure-7d), as explained and summarized in Figure-8. It is worthy to mention that transmission electron microscopy (TEM) technique is better suited for microstructural investigation due to the much higher magnification and resolution abilities [16]. This issue can be assumed as a limitation in this study.

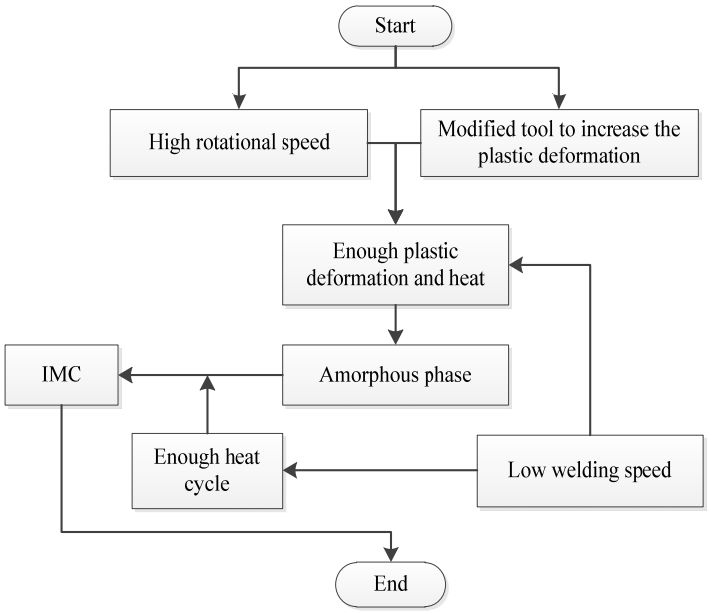

Figure-8. Amorphous phase formation mechanism and its transformation process.

4. CONCLUSIONS

Heat cycle and microstructure have been investigated in this study to evaluate the amorphous phase formation of Al-to- steel joint made by FSW. Remarkable points can be summarized as follows:

a) Amorphous phase is affected by the amount of heat and plastic deformation which resulted from using different welding process parameters. High plastic deformation together with short heat cycle led to this phase as explained by the case of 2000 rpm with 40 mm/min in this study. Though there was high plastic deformation, welding parameters that offer long heat cycle could eliminate the presence of the amorphous phase. For example, using 2000 rpm with 20 mm/min as rotational and welding speeds, respectively, had transformed that amorphous phase into IMCs phase. Therefore, the amorphous phase was not observed with the using of these welding process parameters.

Very high welding speed (300 mm/min) also cannot produce the amorphous phase at the Al-to-steel interface due to the low associated plastic deformation.

b) The types of Al Alloys can also affect the formation process of amorphous phase and the related IMC. At the AA6061 (advancing side), higher amorphous phase is believed to be caused by the higher plastic deformation at that side. Besides, thinner IMC layer was detected at that side for different welding parameters, which can be related to the silicone affinity in this type of Al Alloy.

REFERENCES

[1] Y. Kusuda. 2013. Honda develops robotized FSW technology to weld steel and aluminum and applied it to a mass-production vehicle. Industrial Robot: An International Journal. 40: 208-212.

[2] M. Haghshenas, A. Abdel-Gwad, A.M. Omran, B. Gökc¸ e, S. Sahraeinejad, A.P. Gerlich. 2014. Friction stir weld assisted diffusion bonding of 5754 aluminum alloy to coated high strength steels, Material and Design. 55: 442-449.

[3] H. Springer, A. Kostka, J.F. dos SANTOS, D. Raabe. 2011. Influence of intermetallic phases and Kirkendall-porosity on the mechanical properties of joints between steel and aluminium alloys. Materials Science and Engineering A. 528: 4630-4642.

[4] T. Ogura, Y. Saito, T. Nishida, H. Nishida, T. Yoshida, N. Omichi, M. Fujimoto, A. Hirose. 2012. Partitioning evaluation of mechanical properties and the interfacial microstructure in a friction stir welded aluminum alloy / stainless steel lap joint. Scripta Materialia. 66: 531-534.

[5] Y.F. Sun, H. Fujii, N. Takaki, Y. Okitsu. 2013. Microstructure and mechanical properties of dissimilar Al alloy/steel joints prepared by a flat spot friction stir welding technique. Materials and Design. 47: 350-357.

[6] K.K. Ramachandran, N. Murugan, S. Shashi Kumar. 2015. Effect of tool axis offset and geometry of tool pin profile on the characteristics of friction stir welded dissimilar joints of aluminum alloy AA5052 and HSLA steel. Materials Science and Engineering A. 639: 219-233.

[7] X. Fei, X. Jin, Y. Ye, T. Xiu, H. Yang. 2016. Effect of pre-hole offset on the property of the joint during laser-assisted friction stir welding of dissimilar metals steel and aluminum alloys. Materials Science and Engineering A. 653: 43-52.

[8] S.A. Hussein, S. Thiru, R. Izamshah, A.S.M. Tahir. 2014. Unstable Temperature Distribution in Friction Stir Welding. Advances in Materials Science and Engineering. p. 8, Article ID 980636, http://dx.doi.org/10.1155/2014/980636.

[9] Ø.Frigaard, Ø.Grong, O.T. Midling. 2001. A process model for friction stir welding of age hardening aluminum alloys, Metallurgical and Materials Transactions A. 32A: 1189-1200.

[10] G. C¸am, S. Mistikoglu. 2014. Recent developments in friction stir welding of Al-Alloys. Journal of Materials Engineering and Performance. 23(6): 1936-1953.

[11] D. Jacquin, B. de Meester, A. Simar,D. Deloison, F. Montheillet, C. Desrayaud. 2011. A simple Eulerian thermomechanical modeling of friction stir welding,Journal of Materials Processing Technology. 211: 57-65.

[12] R. Nandan, G.G. Roy, T.J. Lienert, T. Debroy. 2007. Three-dimensional heat and material flow during friction stir welding of mild steel, Acta Materialia. 55: 883-895.

[13] S. Kobayashi, T. Yakou. 2002. Control of intermetallic compound layers at interface between steel and aluminum by diffusion-treatment, Materials Science and Engineering A. 338: 44-53.

[14] D. Rao, K. Huber, J. Heerens, J.F. dos Santos, N. Huber. 2013. Asymmetric mechanical properties and tensile behaviour prediction of aluminium alloy 5083 friction stir welding joints, Materials Science and Engineering A. 565: 44-50.

[15] H. J. Liu, J.C. Hou,H. Guo. 2013. Effect of welding speed on microstructure and mechanical properties of self-reacting friction stir welded 6061-T6 aluminum alloy, Materials and Design. 50: 872-878.

[16] M. Girard, B. Huneau, C. Genevois, X. Sauvage, G. 2010. Racineux Friction stir diffusion bonding of dissimilar metals. Science and Technology of Welding and Joining. 15(8): 661-665.